

Synthesis, Growth and Quantum Analysis on Chloroisocytosine Bromo Methylisocytosine single Crystal

N.Rajeswari^a, R. Santhakumari^{a*}

^aDepartment of Physics, Government Arts College for Women, (Autonomous), Pudukkottai-622 001, (Affiliated to Bharathidasan University, Tiruchrappalli-620 024) Tamil Nadu, India

*Corresponding author email: santhasrinithi@yahoo.co.in

Article Info

Volume 83

Page Number: 295 - 306

Publication Issue:

November/December 2020

Abstract

A slow evaporation approach was used to synthesize an organic crystal chloroisocytosine bromo methylisocytosine (CCBM). The FT-IR spectra of the synthesized crystal were examined to identify several functional groups. UV-Vis-NIR spectroscopy studies were used to assess the crystal's efficiency for optical applications. The findings of theoretical calculations using density functional theory (DFT) were compared to experimental data in order to determine optical geometry using B3LYP with 6-311++G (d, p) basis set. Hirshfeld surface evaluation was used to study into the intermolecular interactions that present inside the crystal.

Keywords: crystal growth; growth from solution; DFT; Hirshfeld surface;

Article History

Article Received : 25 October 2020

Revised: 22 November 2020

Accepted: 10 December 2020

Publication 31 December 2020

1. Introduction

Researchers' interest in various natural materials has increased rapidly in recent years, making it possible to grow efficient organic crystals. Organic crystals are essential in telecommunications, frequency doubling, and optical computing because they perform as a source in electro-optics [1-5]. In organic crystals, the strength of van der Waals interactions is more important than intramolecular chemical bonds for intermolecular attraction in the lattice. Organic nonlinear optical materials have received a lot of attention recently because of their benefits

over inorganic materials. It goes without saying that a crystal developed with a non-centrosymmetry space group will have a strong SHG (second harmonic generation) and non-zero hyperpolarizability [6]. However, according to certain studies, SHG is achievable even in crystals with centrosymmetry space groups and delocalized electrons. This will give the crystal asymmetric polarizability, which will boost the SHG effect [7, 8]. In addition, in centrosymmetry crystals. Furthermore, the presence of hydrogen bonding interactions in centrosymmetry crystals improves the crystal's

thermal and mechanical properties. Single crystal X-ray diffraction research confirms the hydrogen bonding interaction in organic crystals [9, 12]. Based on the preceding literature review, the physical features of chloroisocytosine bromo methylisocytosine (CCBM) have been identified using a variety of characterisation methods.

2. Synthesis and crystal growth

Chloroisocytosine and bromo methylisocytosine are dissolved in N-N dimethylacetamide in a 1:1 ratio to form CCBM. To obtain a homogeneous solution, the mixed solution was continuously stirred

for 1 hour using a magnetic stirrer. For slow evaporation, the solution was filtered into a beaker and preserved in a dust-free condition. Small needle-shaped seed crystals were observed at the bottom of the beaker after 15 days. A saturated solution of CCBM in a 100 mL beaker was used to develop a bulk crystal of CCBM, and one of the most well-shaped seed crystals was placed into the solution. To avoid multiple nucleation, the beaker is covered with a polythene sheet and retained in an undisturbed environment. After a 25-day period, a 9mm x 7mm x 1mm CCBM crystal was obtained.



Figure.1.As grown single crystal of CCBM.

3. Results and discussion

3.1. Powder X-ray diffraction studies

Using powder X-ray diffraction analysis, the calculated lattice parameters $a=9.270$ (5) Å, $b = 11.423$ (4) Å and $c = 12.599$ (7)Å with space group $P2_1/n$ are found to be in good agreement

with the reported value [13]. The powder X-ray diffraction pattern was indexed and compared with the stimulated single crystal diffraction (Mercury 3.0 software) pattern which reveals the exact identity of the grown CCBM crystal.

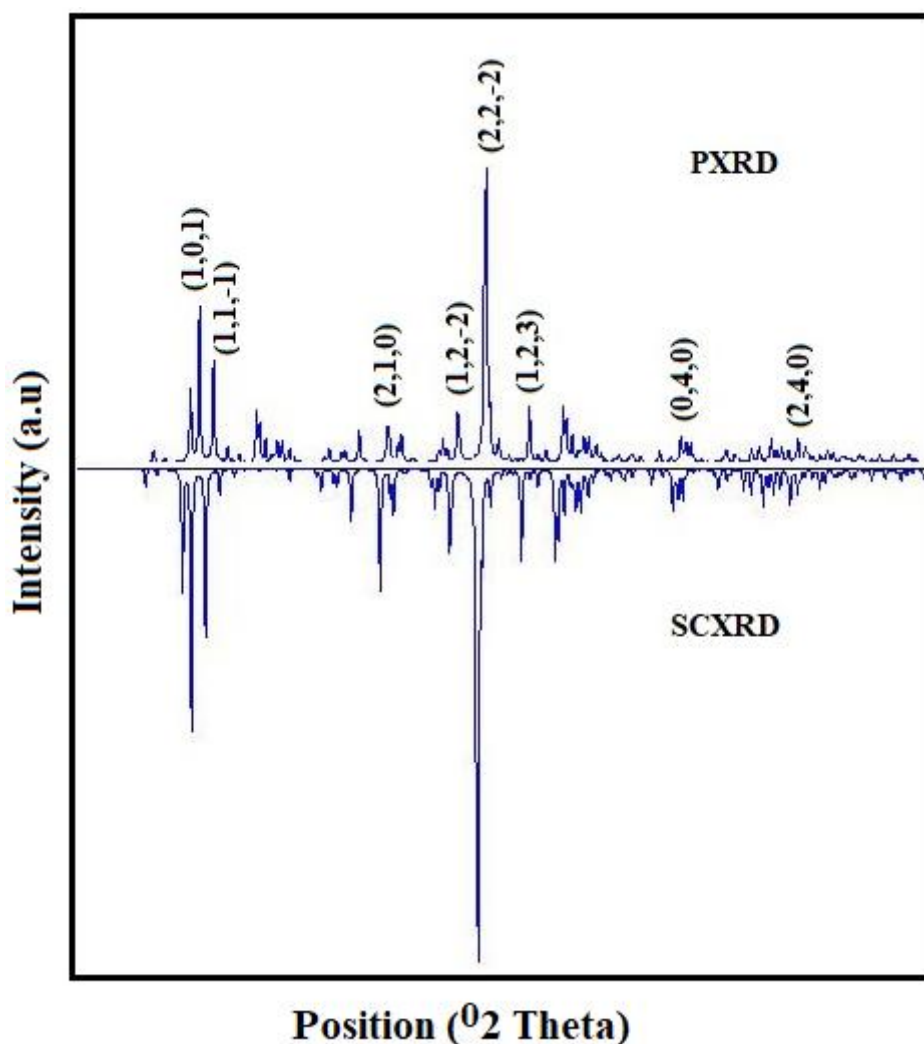


Figure.2. PXRD data of the CCBM generated using the Mercury 3.0 program.

3.2. FT-IR spectral analysis for CCBM

Confirmation of functional groups were done through Fourier Transform Infrared spectrophotometer (FT-IR) and the spectrum was recorded in the range of $4000-500\text{ cm}^{-1}$. The experimental and theoretical spectrum of

FT-IR are shown in Figure.3. The vibrational modes with the theoretical support of PED (potential energy distribution) using VEDA program contribution of 99% are stacked in Table 1.

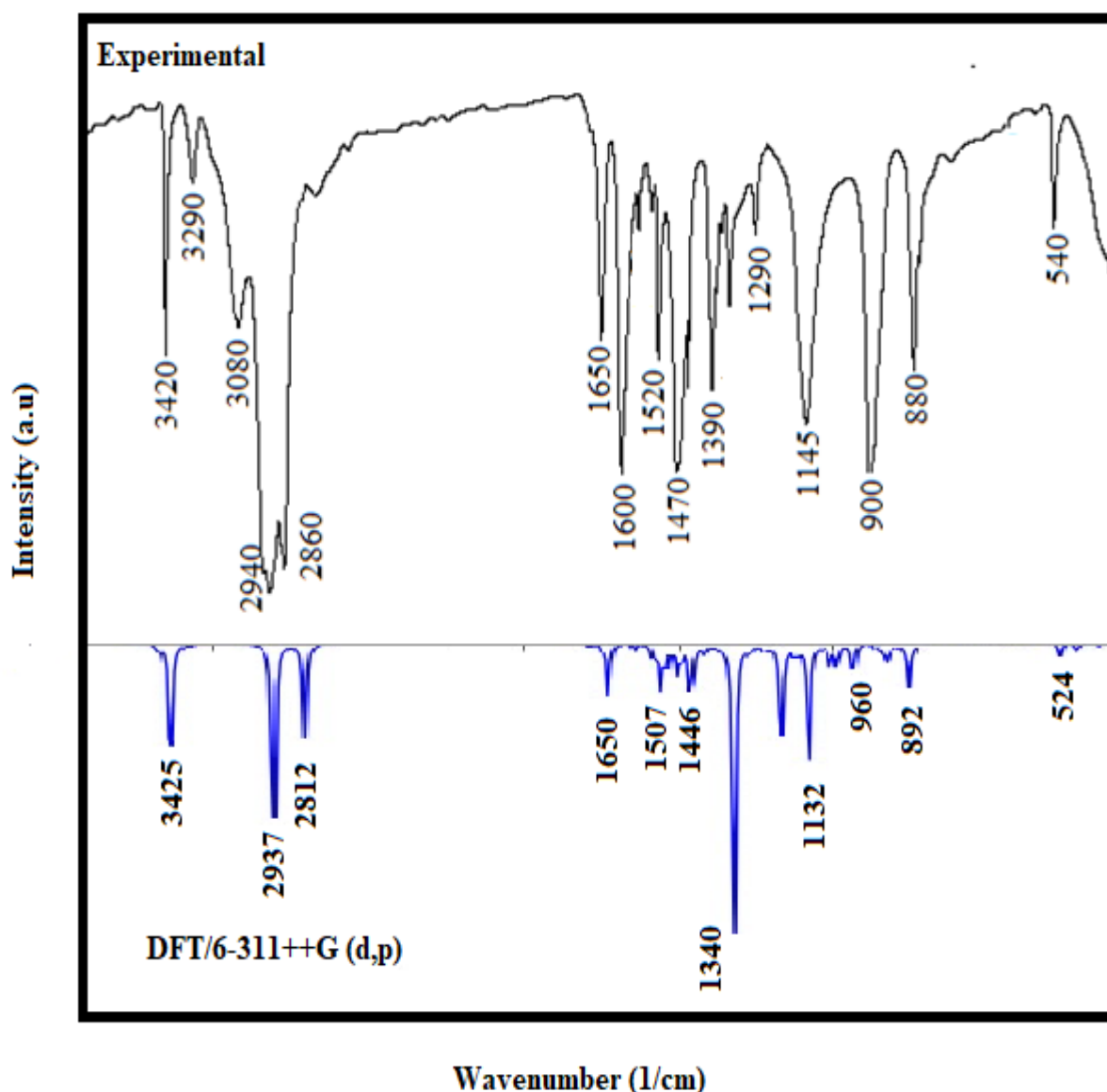


Figure.3.Observed and stimulated FT-IR spectrum of CCBM crystal.

Table1. FT-IR observed and DFT spectral band assignment of CCBM single crystal

Experimental	Theoretical	Assignment with PED (%)
3420	3425	ν_s N-H (99)
2940	2937	ν_s C-H (98)
2860	2812	ν_s C-H (97)
1650	1650	ν_s C=O (94)
1520	1507	ν_s C=N (92) and τ C-H (87)
1470	1446	ν_s C=C (77), δ_{ip} C-H (66), and ω O-H (63)
1390	1340	ν_s C=C (72)
1145	1132	γ C-H (68)
900	960	ρ C-H (71)
880	892	τ C-H (66)
540	524	ν_s C-Br (84)

ν_s – symmetric stretching; ν_{as} – asymmetric stretching; β – in-plane bending; γ – out-plane bending; δ – scissoring; δ_{ip} – scissoring in-plane; δ_{op} – scissoring out-plane; τ – twisting; ω – wagging; ρ – rocking.

3.3. UV-vis-NIR spectral studies

The optical characteristics of the CCBM crystal were examined using a SHIMADZU (UV-2600) spectrophotometer, and a spectrum in the region of 200-800 nm was acquired. The crystal examined in this investigation has a thickness of 2mm. The production of single crystal CCBM was detected by comparing the experimental spectrum to the theoretical spectrum in different solvents using TDB3LYP (Time dependent density functional theory) at the 6-311++G(d,p) basis

set. The prominent peak at 404.62 nm with oscillator strength (f) of 0.0023 is attributable to charge transfer to the excited singlet state S0-S1, according to the theoretical calculation. Table 2 shows the theoretical and experimental maximum values. The spectra were taken in gas and various solvents (Acetone and Methanol), as shown in Figure 4. Because of the solvent effect, the absorption peaks in all other solvents showed modest changes compared to gaseous state.

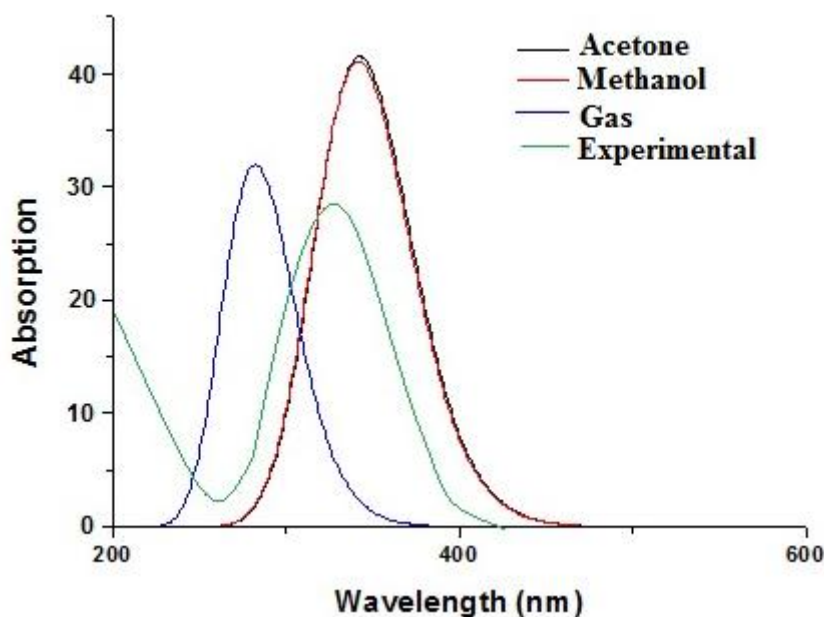


Figure 4. Experimental and Theoretical UV spectrum (Recorded by TD-SCF/DFT/B3LYP/6-311 G(d,p)in different solvents) of CCBM single crystal.

Table 2: Experimental and calculated electronic transition parameters of CCBM by TDSCF/DFT/B3LYP/6-311 G(d,p)method in gas and other solvents.

Solvent	Spec trum	Electronic Transition	E _t	λ _{max}		F	ε (%)
				Experiment al	Calculated		
Gas	UV	Excited state I H-L (H-1)-L	3.5601	331	404.62	0.0023	96 20
		Excited state II H-L (H-1)-L	3.4884		353.40	0.2801	97
		Excited state III H-L (H-1)-L	3.6510		336.74	0.5414	72 23
ACETONE	UV	Excited state I H-L (H-1)-L	3.5274		351.55	0.0531	96 17
		Excited state II H-L	3.6158		342.80	0.9172	97
		Excited state III H-L (H-1)-L	3.9489		315.59	0.1027	74 22
METHANOL	UV	Excited state I H-L (H-1)-L	3.5326		349.11	0.0639	96 18
		Excited state II H-L	3.6423		343.12	0.8967	97
		Excited state III H-L (H-1)-L	3.9527		314.37	0.1041	72 23

*H-HOMO, L-LUMO

E_t – Transition energy (eV)

λ_{max} – Electronic absorption wavelength (nm)

f – Oscillator strength

ε - Contribution (%)

3.4. HOMO - LUMO analysis

HOMO-LUMO analysis were carried out using B3LYP 6311++G(d,p) basis sets and the energy gaps are depicted in Figure 5. The HOMO and LUMO are the most important aspects of quantum chemistry which explains the role of electron donor and acceptor respectively [14]. E_{HOMO}

(highest occupied molecular orbital) and E_{LUMO} (lowest unoccupied molecular orbital) values are -0.20246 a.u and -0.03756 a.u, respectively. The estimated energy gap is 4.4871 eV. The values indicates that the CCBM molecules are highly efficient in electrical activity.

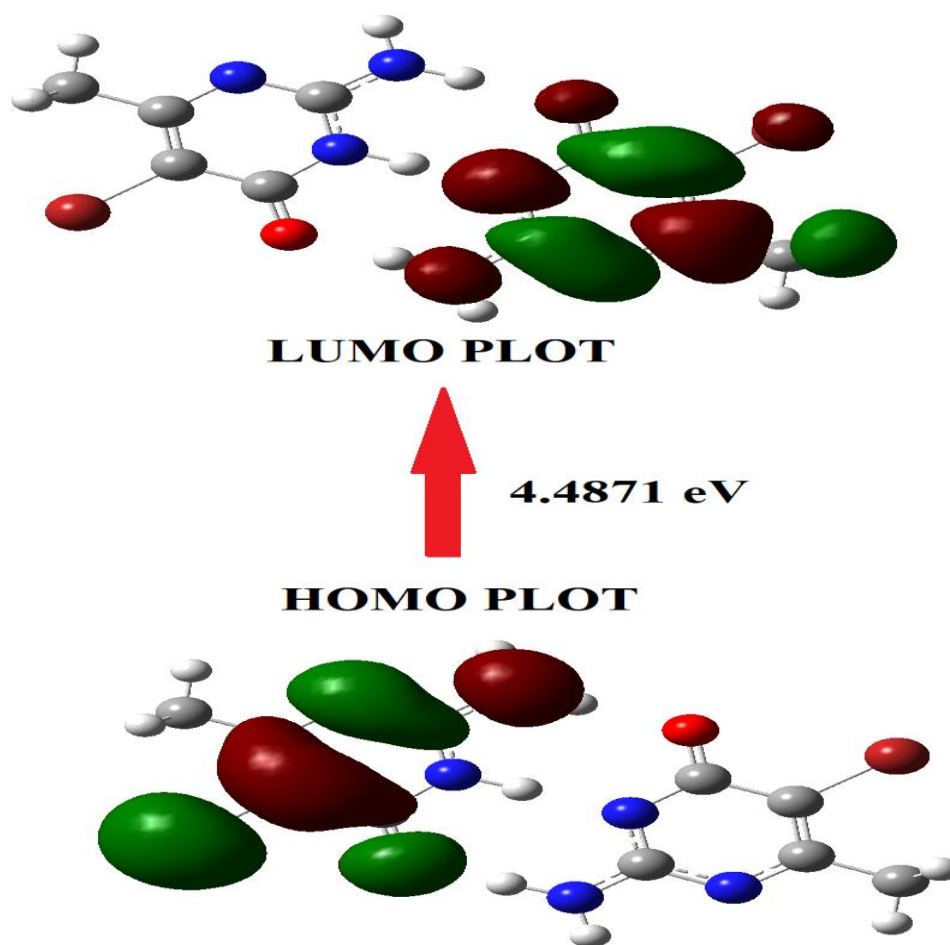


Figure 5. HOMO – LUMO plot of CCBM

3.5. Molecular electrostatic potential (MEP)

From DFT studies it is revealed that the electrostatic potential depicted in Figure 6 ranges from -6.260 to $+6.260$ a.u. represents

the deepest blue density which in turn gives the electron deficient region, $V(r) > 6.260$ a.u. and deepest red density represents the electron rich region $V(r) < -6.260$ a.u.

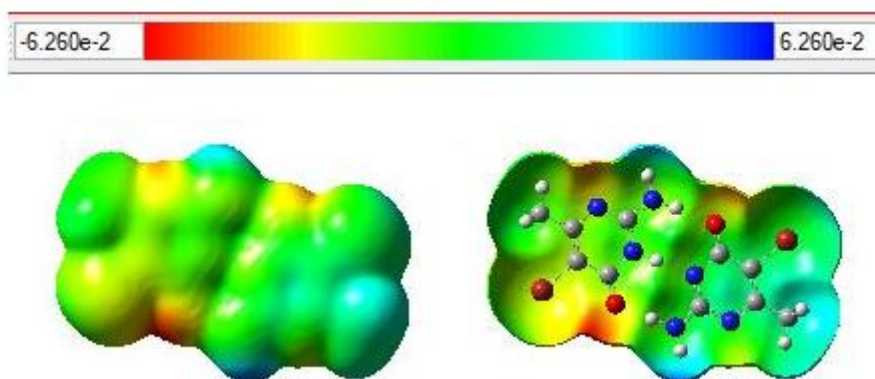


Figure 6. Calculated 3D molecular electrostatic potential contour map of CCBM.

3.6. Mulliken population analysis (MPA) and Natural population analysis (NPA)

The following charge distributions on several atoms (C, H, and O) are obtained using Mulliken population analysis (MPA) and Natural population analysis (NPA) using the B3LYP/6-311++G(d,p) method. Figure 7 shows a study of Mulliken atomic charges and Natural atomic charges utilising the B3LYP/6-

311++G(d,p) approach for CPM (cluster partitioning method). When hydrogen or oxygen enters the picture, the carbon atom becomes more electron-deficient. Bromine atoms and all hydrogen atoms have positive charges. Each of the carbon atoms has a negative charge. The Br atom has a greater positive charge of 0.099828 than ordinary hydrogen atoms due to the presence of oxygen and carbon atoms on both sides.

Table 3. Mulliken Atomic Charge and Natural Atomic Charge of CCBM

Atoms	MPA	NPA	Atoms	MPA	NPA
1 N	0.034953	0.033873	17 C	-0.043632	-0.361173
2 C	-0.007724	-0.185358	18 N	0.154308	0.203760
3 N	0.023322	-0.148744	19 H	-0.006208	0.010628
4 H	-0.002653	-0.161571	20 H	-0.005166	0.001573
5 H	-0.000953	0.287118	21 N	-0.018871	-0.329137
6 N	-0.002121	-0.266611	22 C	-0.085622	-0.378531
7 C	-0.011841	0.014197	23 O	0.164272	0.037284
8 O	0.022009	-0.201032	24 C	0.480105	0.659280
9 C	0.053548	0.203956	25 Br	0.099828	0.391219
10 Br	0.016899	0.434244	26 C	-0.142207	0.456726
11 C	-0.015756	0.753012	27 H	-0.000993	-0.000839
12 C	0.001023	-0.086074	28 H	-0.003695	-0.006539
13 H	-0.000119	0.042883	29 H	-0.003695	0.002853
14 H	-0.000392	0.013452	30 C	0.009086	0.003667
15 H	-0.000392	0.013482	31 H	0.000136	0.000681
16 N	0.292552	0.380796			

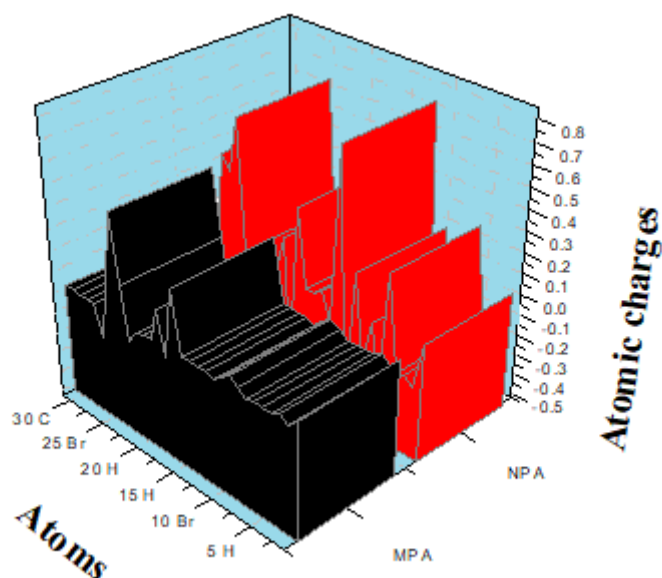


Figure 7. Mulliken population analysis and Natural population analysis

3.7. Natural Bond Orbital Analysis

At the B3LYP/6-311++G(d,p) level, NBO analysis was performed on the CCBM molecule to define the intramolecular hybridization and delocalization of electron density within the molecules. Intramolecular hyper conjugative interactions are formed by overlapping the orbitals between bonding (N-C) and (C-C) orbitals, as well as the anti-

bonding (N-C) and (C-C) orbitals, resulting in intramolecular charge transfer (ICT), which stabilises the molecular system and increases electron density [15]. The significant interactions between Lewis and non-Lewis orbitals are shown in Table 4. The interaction between the oxygen and nitrogen lone pair of the $n_3(O_8)$, $n_1(N_3)$ to antibonding (N6-C7), (N1-C2) gives the strong stabilisation energy (93.25 and 39.44 KJmol^{-1}).

Table 4. Second-order perturbation theory analysis of Fock matrix in NBO basis of CCBM single crystal

Donor(i)	ED/e	Acceptor(j)	ED/e	$E(2)^a(\text{K J mol}^{-1})$	$E(i)-E(j)^b(\text{a.u})$	$F(i,j)^c(\text{a.u})$
$\pi(N1-C2)$	0.82206	$\pi^*(C9-C11)$	0.16490	13.50	0.30	0.082
$\pi(N6-C7)$	0.90144	$\pi^*(N1-C2)$	0.25031	18.67	0.32	0.106
$\pi(C9-C11)$	0.85994	$\pi^*(N6-C7)$	0.02694	14.66	0.21	0.078
$n_1(N_3)$	0.80799	$\pi^*(N1-C2)$	0.25031	39.44	0.21	0.19
$n_3(O_8)$	0.73120	$\pi^*(N6-C7)$	0.02694	93.25	0.15	0.157

n2(O8)	0.91330	$\sigma^*(N3-H4)$	0.05328	18.63	0.69	0.147
--------	---------	-------------------	---------	-------	------	-------

^aE(2) means energy of hyperconjugative interactions

^bEnergy difference between donor and acceptor NBO

^cF(i,j^{''}) is the Fock matrix element between the donor and acceptor NBO.

3.8. Hirshfeld surface analysis

The Hirshfeld surface (HS) analysis was carried out to study about the intermolecular interactions in the crystal. The d_{norm} , d_{norm} transparency and shape-index surface supports the presence of N–H...O and N–H...N intramolecular interactions in the structure of CCBM (Figures 8a, 8b and 8c). Figure.9 shows the 2D fingerprint plots

reveals that the greatest contribution to the Hirshfeld surfaces is from H...H contacts, followed by H...O/O...H contacts. In the title compound, the H...H (26.2%) has highest contribution, then Br...H (12.9%), H...Br (7.6%), H...O (6.5%), N...H (6.2%) and C...H (4.4%) contributions.

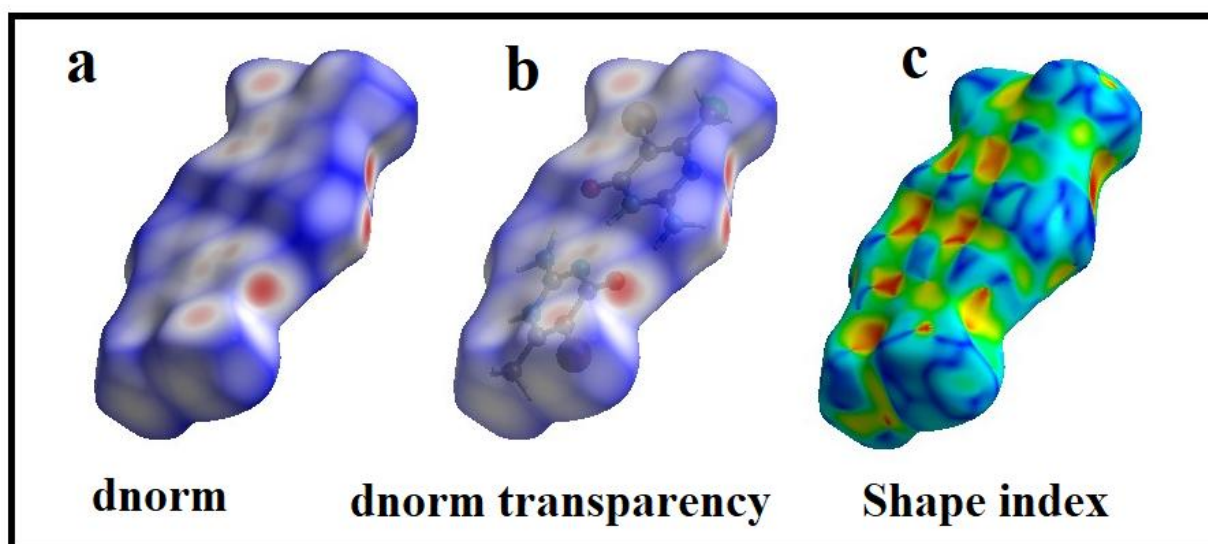


Figure. 8. Intermolecular interaction.

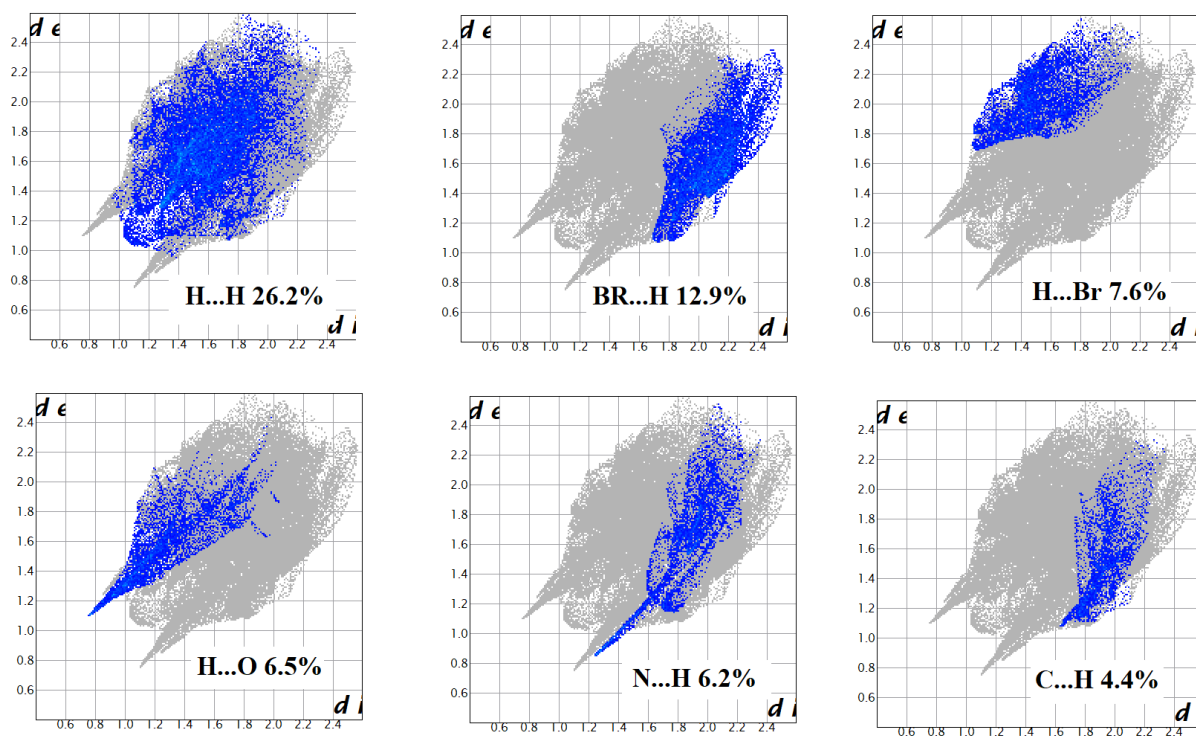


Figure. 9.2-D fingerprint plots.

4. Conclusions

chloroisocytosine bromo methylisocytosine has been grown at room temperature using slow evaporation technique. Powder X-ray diffraction, FT-IR, and UV- vis-NIR studies confirms the formation of crystal structure with the calculated cell parameters, presence of functional groups and optical absorption. Since the crystal has 4.4871 eV as energy gap which predicts that it is suitable for electrical conductivity process. The charge transfer is taking place within the molecule which was revealed by HOMO-LUMO analysis. NBO, MEP and Hirshfeld surface analyses of the crystal are good evidence for the stability of crystal structure through intermolecular interactions that exist between oxygen and amine groups.

Acknowledgement

One of the authors (RS) thanks the Tamil Nadu State Council for Higher Education for the financial support [File No. D.O.Rc.No.744/2017 A]. The authors thank IIT Madras, Alagappa University, Karaikudi, St. Joseph's college, Tiruchirappalli and SASTRA University, Thanjavur for extending the lab facilities to record the Single XRD, FTIR, and UV-vis-NIR spectra respectively.

References

- [1] Periyasamy B.K., Jebas R.S., Hailampillai B., *Mater. Lett.*, 61 (2007), 1489.
- [2] Munn R.W., Ironside C.W., *Principles and applications of nonlinear optical materials*, CRC Press, Inc., USA, 1994.
- [3] Dalton L.R., Sullivan P.A., Olbrich B.C., Bale D.H., Takayesu J., Hammond S., Rommel H., Robinson B.H., *Tutorials in Complex Photonics Media*, SPIE, Bellingham, WA, 2007.

- [4] Kaino T., Cai B., Takayama K., *Adv. Funct. Mater.*, 12 (2002), 599.
- [5] Bardan J., Hierle R., Perigaud A., Zyss J., Williams D.J., *Nonlinear optical properties of organic molecules and polymeric materials. ACS Series*, Vol. 223, American Chemical Society, Washington DC, 1993.
- [6] Prasad P.N., Williams D.J., *Introduction to Nonlinear Optical Effects in Molecules and Polymers*, Wiley, New York, 1991.
- [7] Rieckhoff, K. E. & Peticolas, W. L. (1965). "Optical second-harmonic generation in crystalline amino acids" *Science*, vol. 147, no. 3658, pp. 610–611.
- [8] Guo, W. Guo, F. & Wei, C. (2002). "SHG from centrosymmetric supermolecular crystal," *Science in China Series B: Chemistry*, vol. 45, no. 3, pp. 267–274.
- [9] Criado, A. Dianez, M. Jerez-Garrido, S. P. Fernandes, I. M. L. Belsley, M. & De Matos Gomes, E. (2000). "1,1,3,3-tetramethylguanidinium dihydrogenorthophosphate," *Acta Crystallographica*, vol. 56, no. 7, pp. 888–889.
- [10] Zaccaro, J. Salvastrini, J. P. Ibanez, A. Ney, P. & Fontana, M. D. J. (2000). "Electric-field frequency dependence of Pockels coefficients in 2-amino-5-nitropyridium dihydrogen phosphate organic-inorganic crystals," *Journal of the Optical Society of America B*, vol. 17, no. 3, pp. 427–432.
- [11] Chandramohan, A. Bharathikannan, R. Kandhaswamy, M. A. Chandrasekaran, J. Renganathan, R. & Kandavelu, V. (2008). "Synthesis, spectral, thermal and NLO properties of N,N-dimethyl anilinium picrate," *Crystal Research and Technology*, vol. 43, no. 2, pp. 173–178.
- [12] Chandramohan, A. Gayathri, D. Velmurugan, D. Ravikumar, K. & Kandhaswamy, M. A. (2007). "1,3,7-Trimethylxanthenium 2,4,6-trinitrophenolate," *Acta Crystallographica Section E*, vol. 63, no. 5, pp. 2495–2496.
- [13] Valeska Gerhardt and Michael Boleb, *Acta Cryst.* (2016), C72, 84-93.
- [14] Roeges N.P., Baas J.M.A, *A Guide to the complete Interpretation of Infrared Spectra of Organic Structures*, Chichester etc., Wiley, 1994, p.282 (f).
- [15]. Glendening E.D., Reed A.E, Carpenter J.E., Weinhold F. NBO version 3.1; University of Wisconsin, Madison, 1999.